Supporting Information

Optimizing d-p Orbital Hybridization by Tuning High-Entropy Spinel Oxides for Enhanced Alkaline OER Efficiency

Dongyuan Song,[1] Xueda Liu,[1] Yingkai Wu,[1] Quan Quan,[2] Yuta Tsuji,[3] Xiaoge Liu,[1] Hikaru Saito,[4] Shiro Ihara,[4] Liyuan Dai,[1] Xiaoguang Liang,[5, 6] Takeshi Yanagida,[4, 7] Johnny C. Ho,[2, 4, 8*] and SenPo Yip[4*]

1 Interdisciplinary Graduate School of Engineering Sciences, Kyushu University, Fukuoka 816-8580, Japan.

2 Department of Materials Science and Engineering, City University of Hong Kong, Hong Kong SAR 999077, China.

3 Faculty of Engineering Sciences, Kyushu University, Kasuga, Fukuoka 816-8580, Japan

4 Institute for Materials Chemistry and Engineering, Kyushu University, Fukuoka 816–8580, Japan.

5 School of Physical Science and Technology, Guangxi Normal University, Guilin 541004, PR China

6 Guangxi Key Laboratory of Low Carbon Energy Materials, Guangxi Normal University, Guilin, 541001 P. R. China

7 Department of Applied Chemistry, Graduate School of Engineering, The University of Tokyo, Tokyo 113-8656, Japan.

8 State Key Laboratory of Terahertz and Millimeter Waves, City University of Hong Kong, Hong Kong SAR 999077, China

*Corresponding authors.

E-mail addresses: johnnyho@cityu.edu.hk and yip.sen.po.472@m.kyushu-u.ac.jp

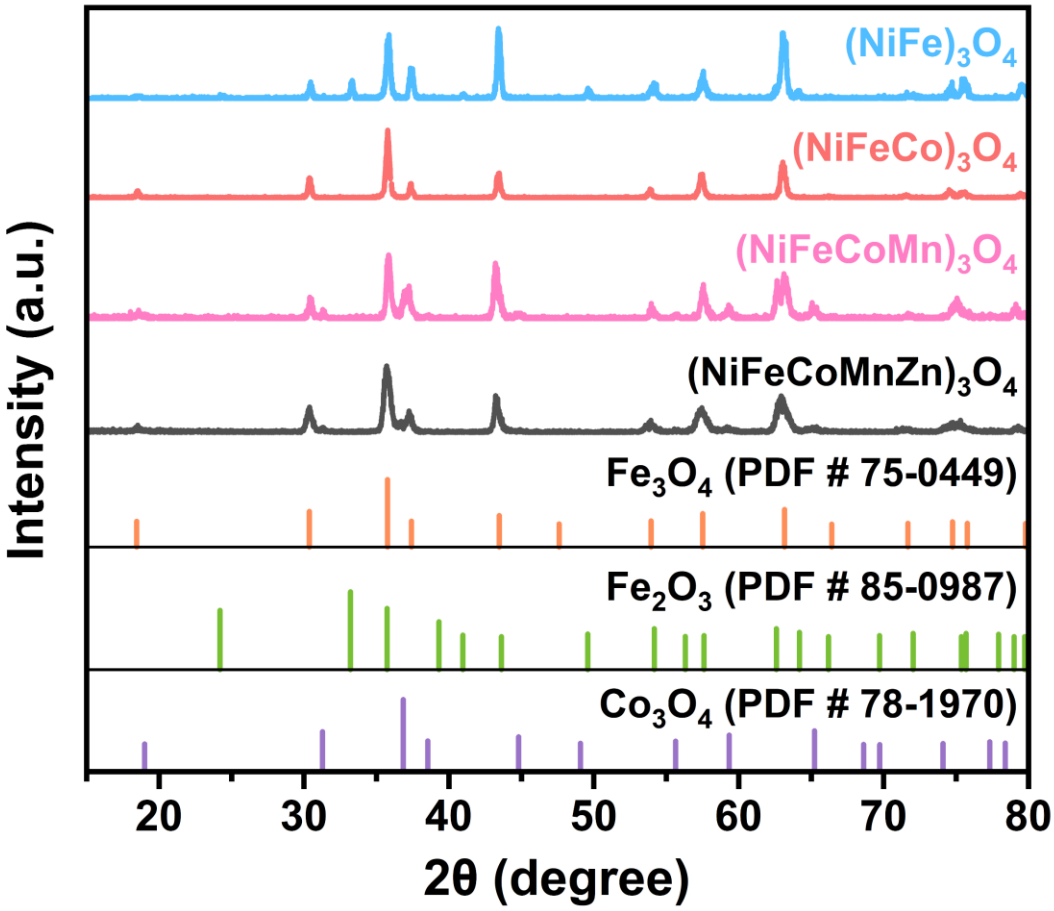

Fig. S1. XRD pattern of equimolar spinel oxides with different degrees of entropy.

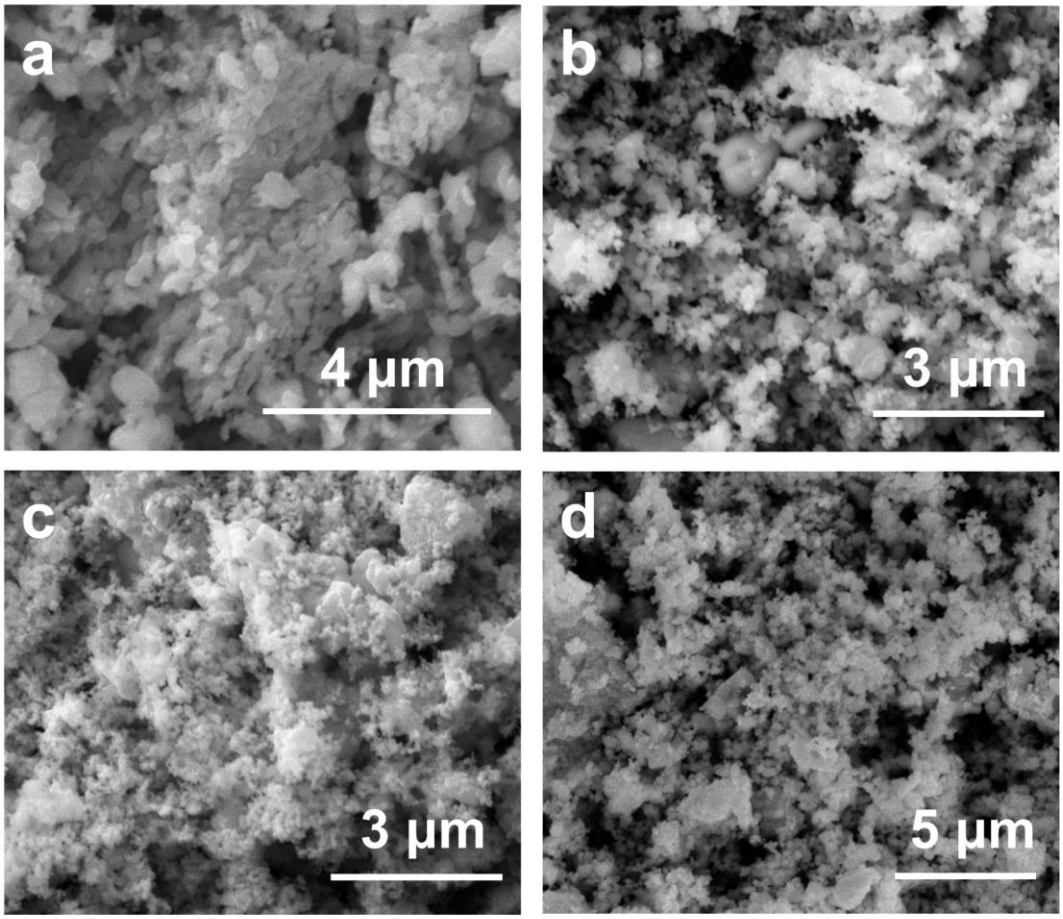

Fig. S2. SEM images of a) $(Ni_{0.5}Fe_{0.5})_3O_4$; b) $(Ni_{0.33}Fe_{0.33}Co_{0.33})_3O_4$; c) $(Ni_{0.25}Fe_{0.25}Co_{0.25}Mn_{0.25})_3O_4$; d) $(Ni_{0.2}Fe_{0.2}Co_{0.2}Mn_{0.2}Zn_{0.2})_3O_4$ sample.

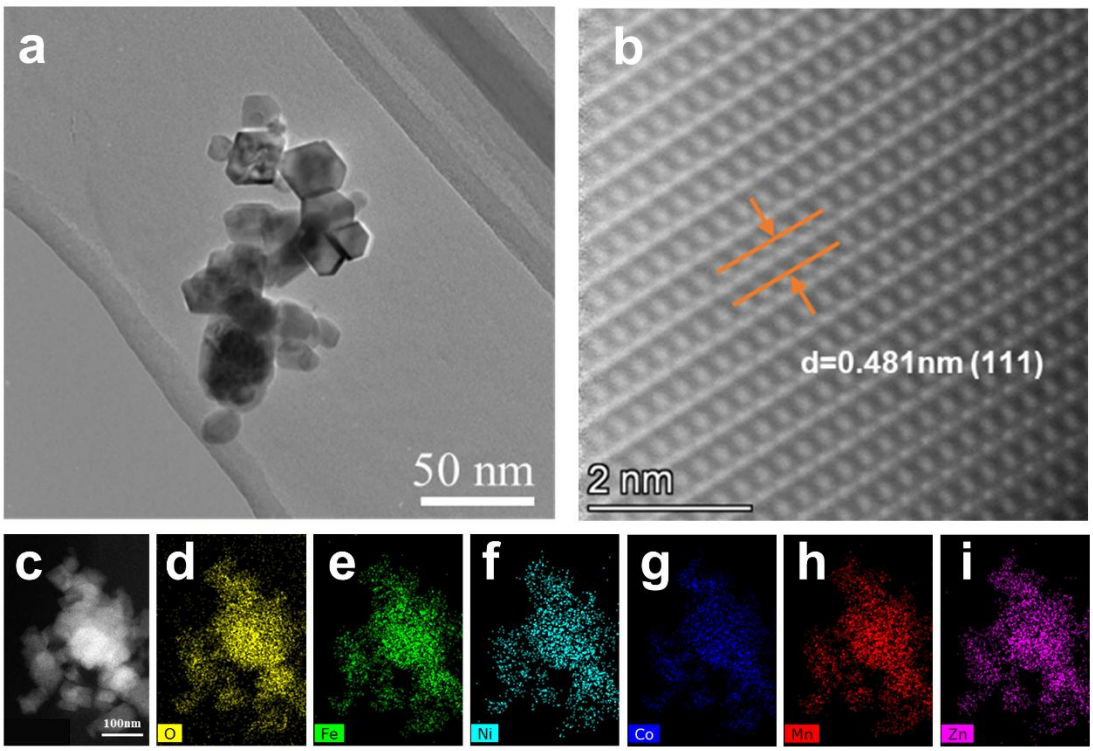

Fig. S3. (a) TEM image of the equimolar HESO sample; (b) Magnified image of a part of (a); (c) Annular dark-field (ADF)-STEM image and (d–i) EDS elemental mappings of O, Fe, Ni, Co, Mn and Zn elements corresponding to (c).

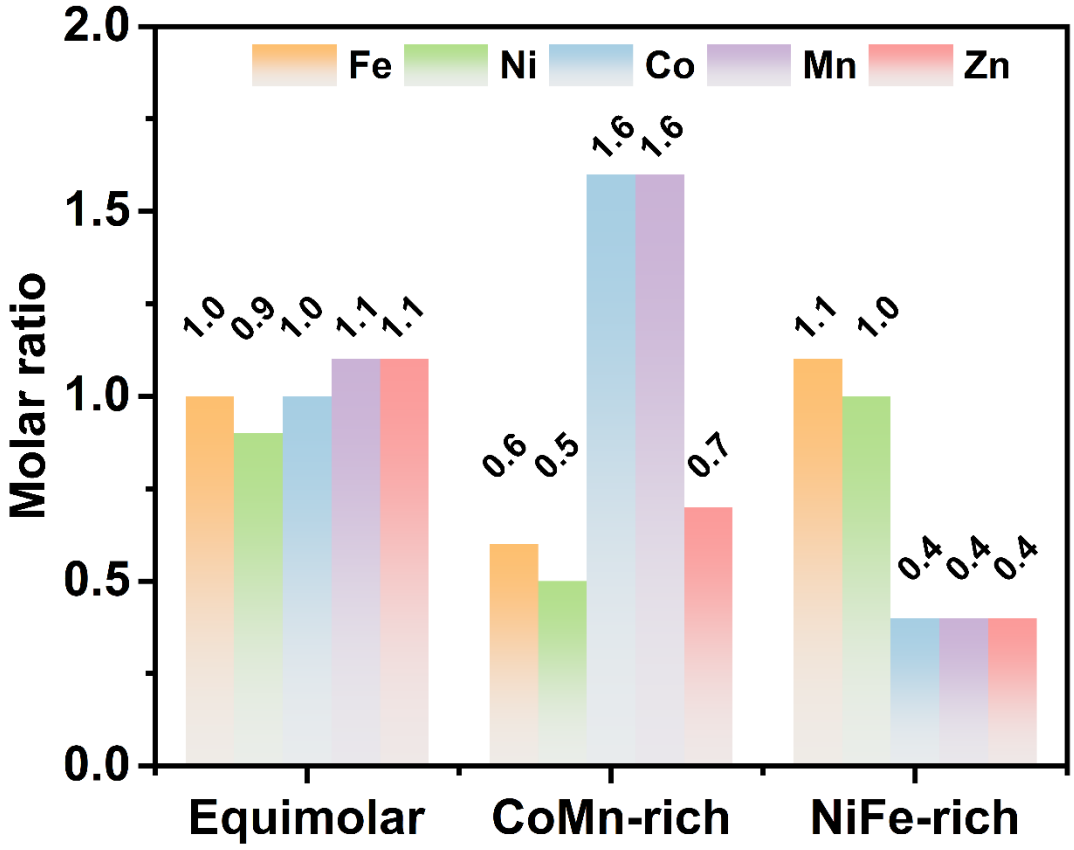

Fig.S4 Element concentration of HESOs determined by ICP-MS results.

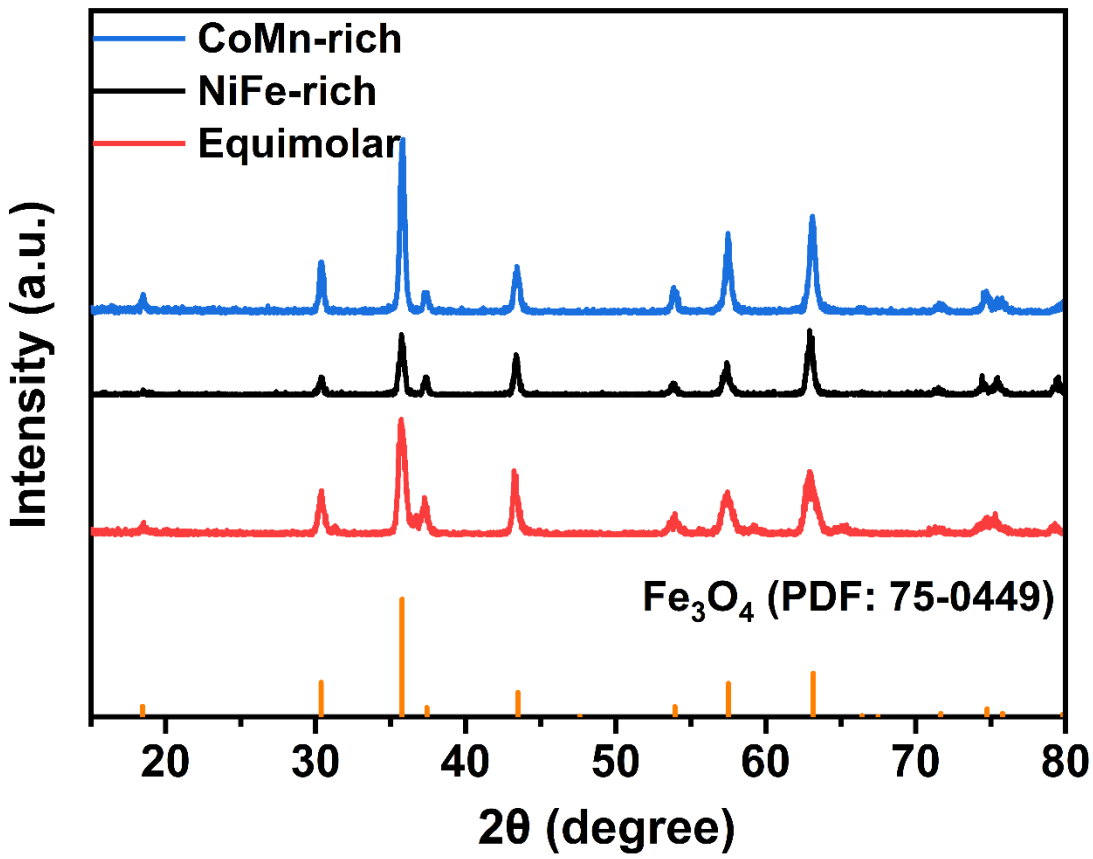

Fig. S5. XRD pattern of the equimolar, CoMn-rich, and NiFe-rich samples.

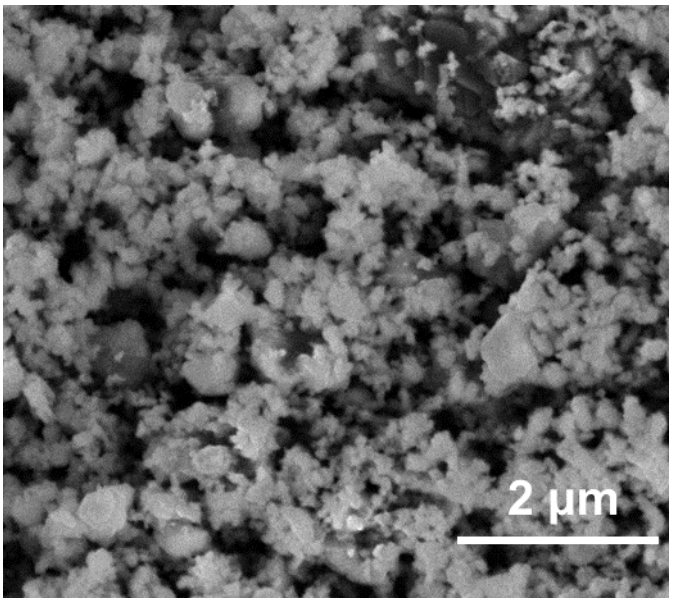

Fig. S6. SEM of the NiFe-rich HESOs.

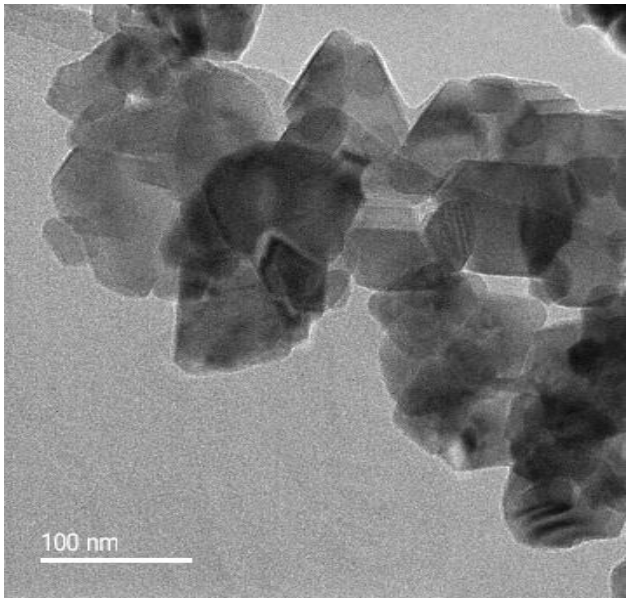

Fig. S7. TEM of the NiFe-rich HESOs.

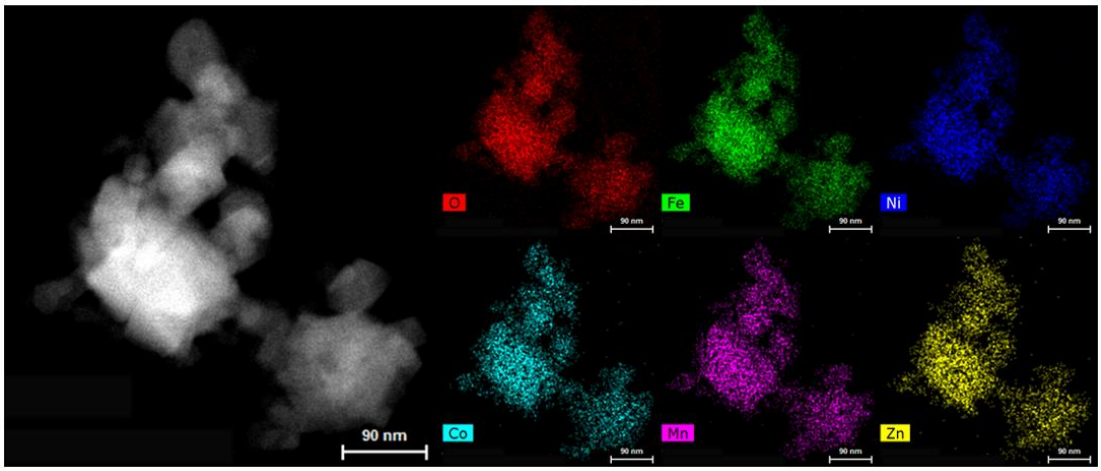

Fig. S8. ADF-STEM image of the NiFe-rich sample and the corresponding elemental mappings of O, Fe, Ni, Co, Mn, and Zn elements.

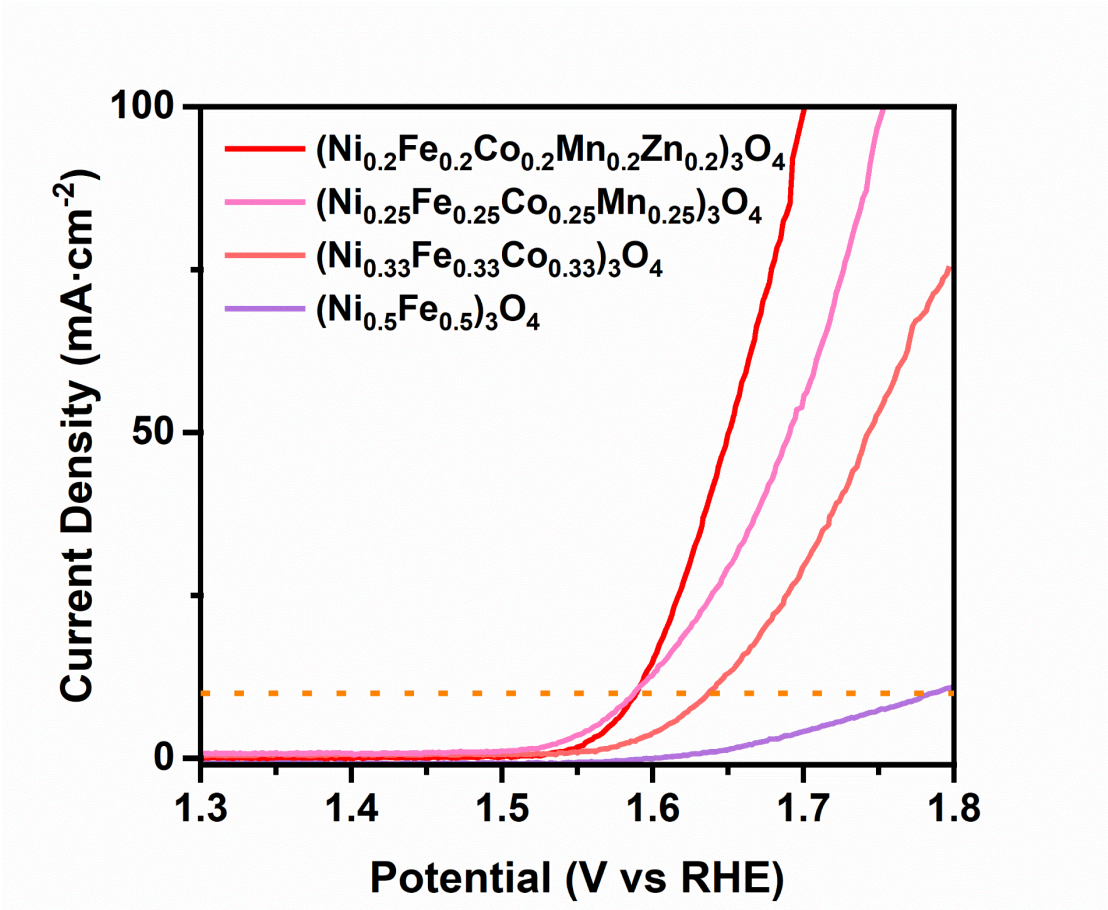

Fig. S9. Comparison of LSV curves for equimolar spinel oxides with different degrees of entropy.

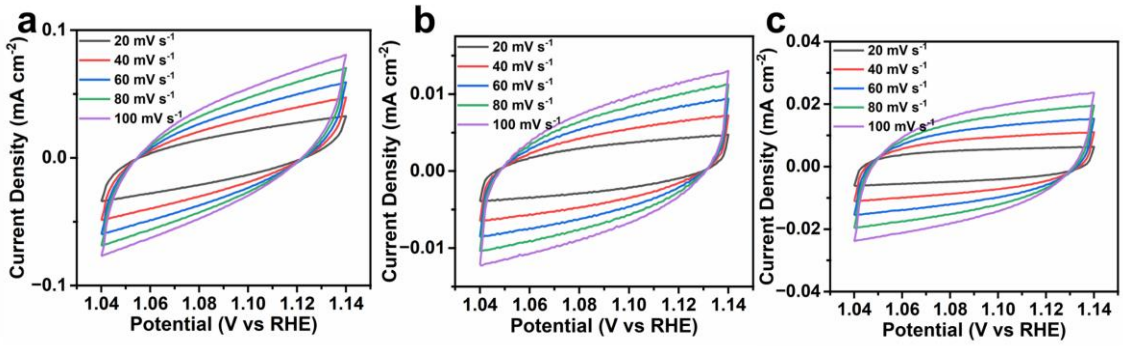

Fig. S10. CV curves of the (a) CoMn-rich, (b) NiFe-rich, and (c) equimolar HESOs at different scan rates from 20-100 mV s^{-1}.

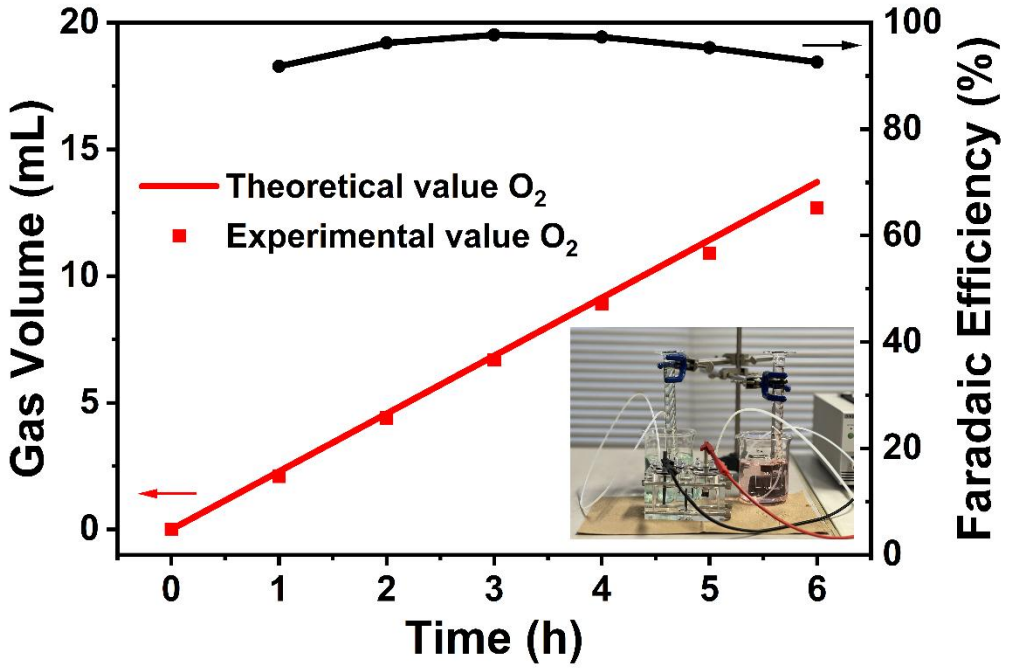

Fig. S11 Theoretical and practical oxygen production and Faradaic efficiency of O2 production (insert: photograph of the device for collecting gas.)

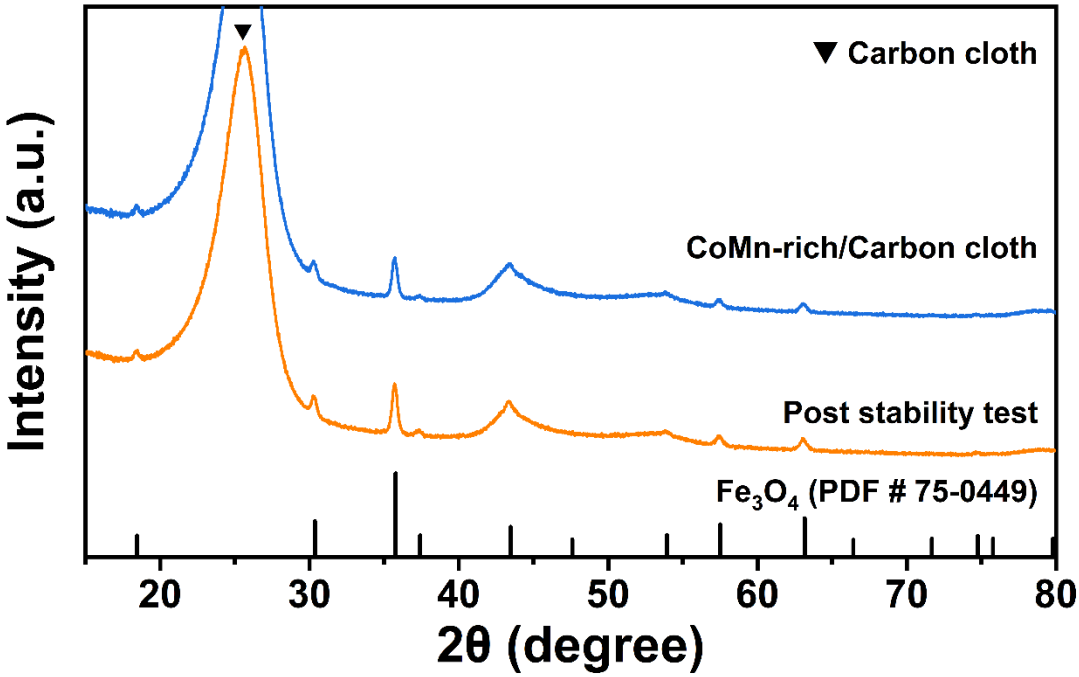

Fig. S12. XRD patterns of CoMn-rich HESO coated on CP.

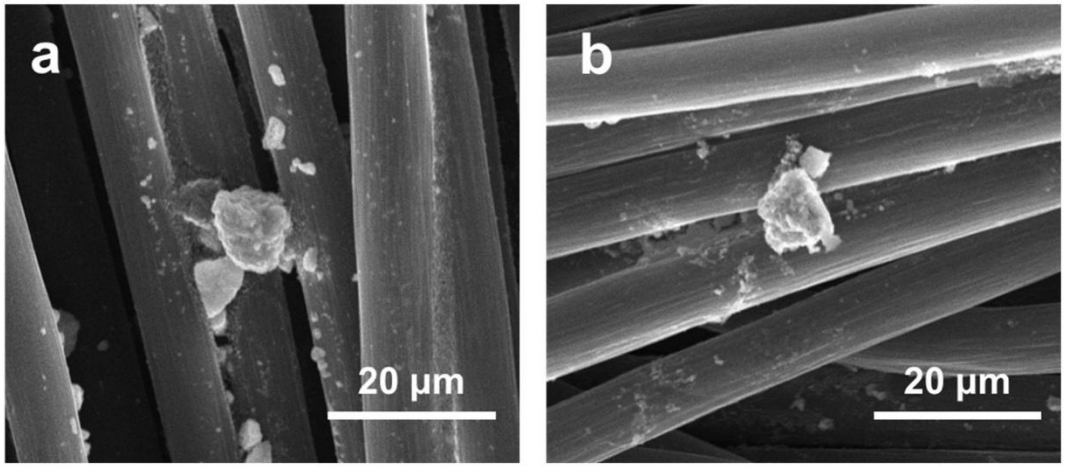

Fig. S13. SEM images of CoMn-rich HESO coated on CP (a) Before the CP test; (b) after the CP test.

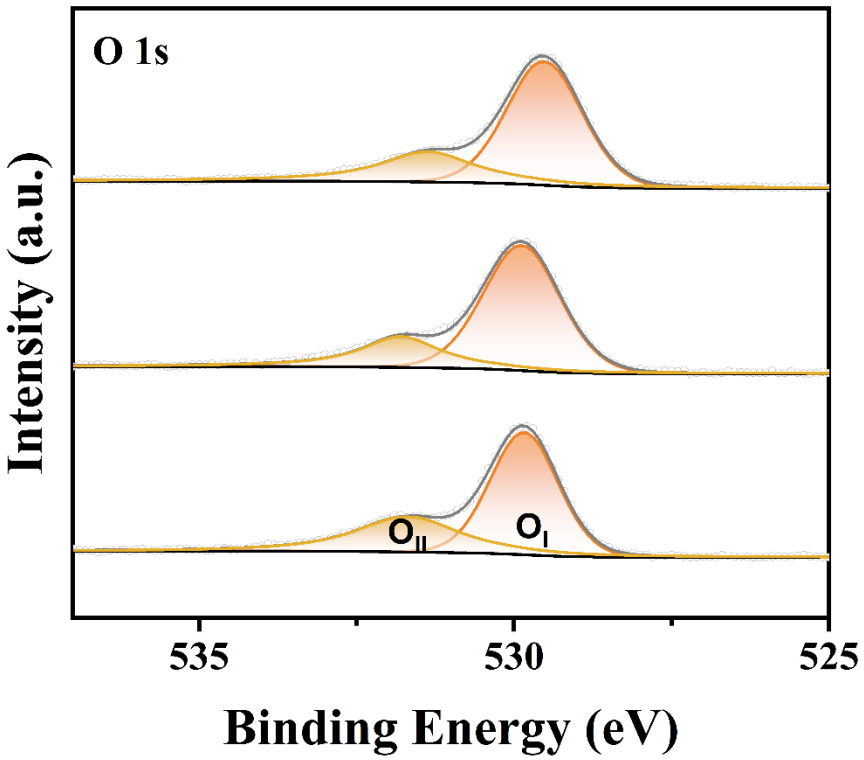

Fig. S14. O 1s spectra of the equimolar, the NiFe-rich, and the CoMn-rich samples after Ar+ sputtering 60s.

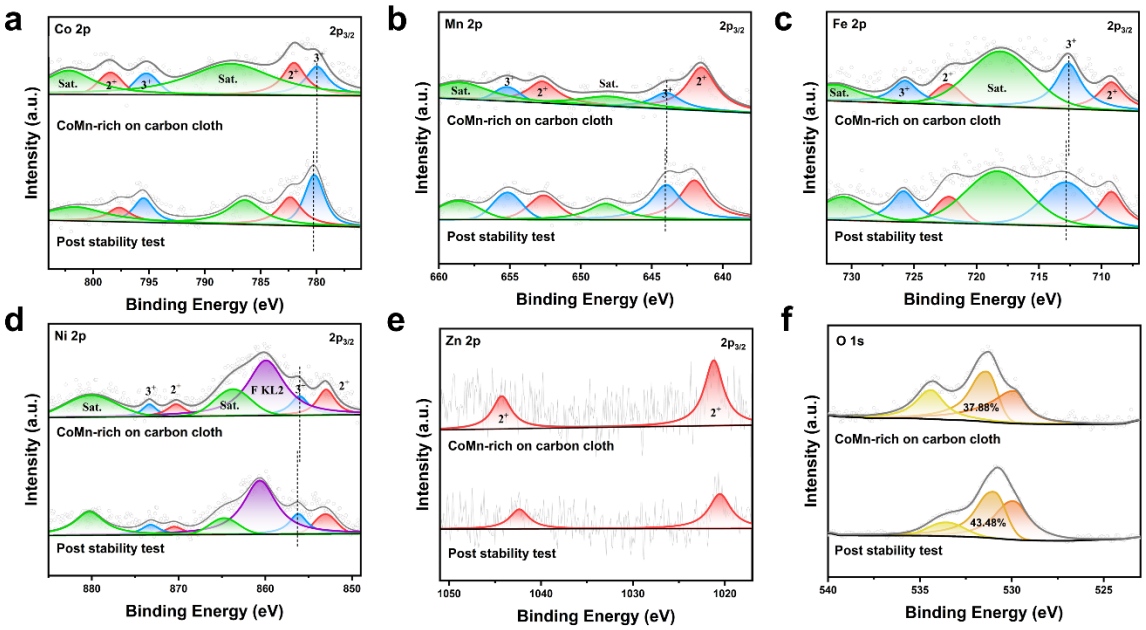

Fig. S15. High-resolution XPS spectra of the CoMn-rich before and after the CP test: (a) Co 2p, (b) Mn 2p, (c) Fe 2p, (d) Ni 2p, (e) Zn 2p, (f) O 1s.

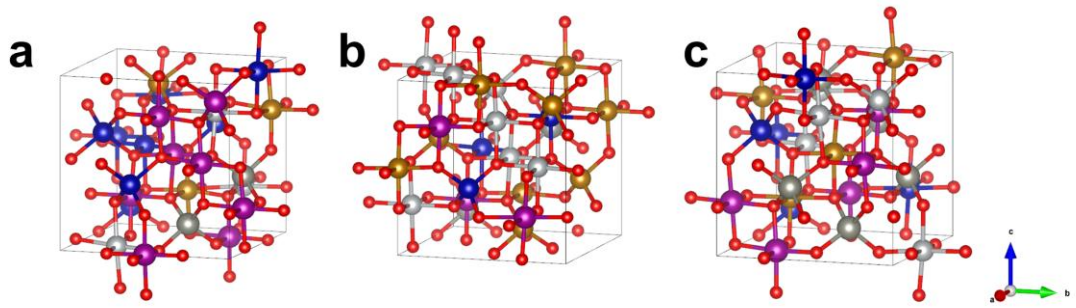

Fig. S16. Stable crystal structures of the a) CoMn-rich, b) NiFe-rich, and c) equimolar HESOs.

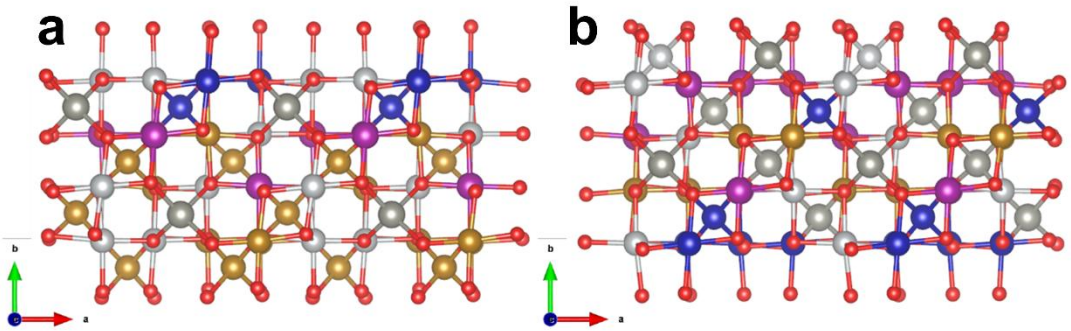

Fig. S17. Top views of the structures of (a) NiFe-rich and (b) equimolar HESOs in (010) plane.

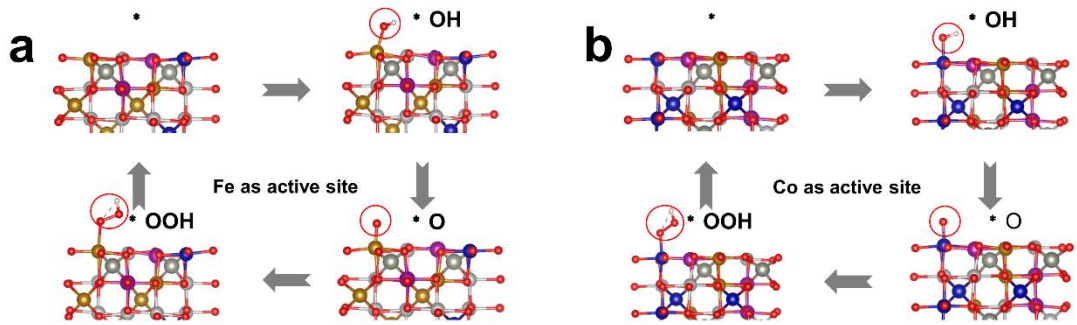

Fig. S18. Side views of adsorption configurations during the OER process on the metal sites of the (a) NiFe-rich and (b) equimolar HESOs.

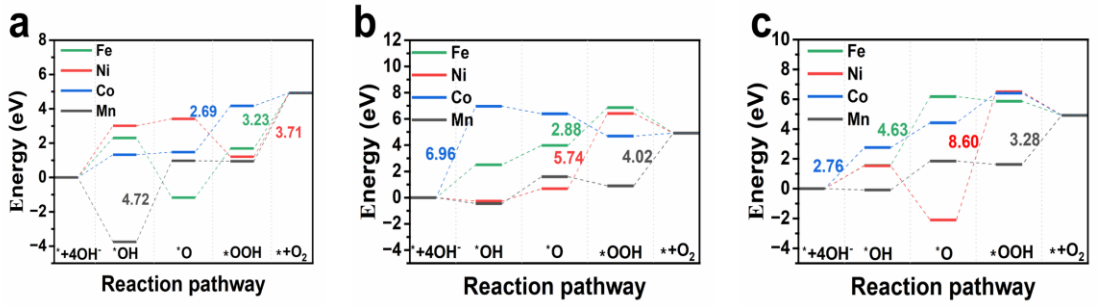

Fig. S19. Energy diagrams of the OER at different metal sites for the a) CoMn-rich, b) NiFe-rich, and c) equimolar HESOs.

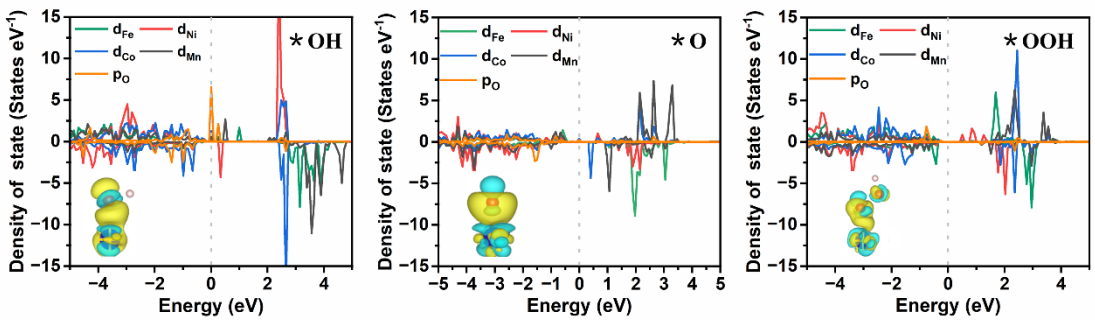

Fig. S20. DOS and charge density difference of the equimolar HESO at *OH, *O, and *OOH adsorption step (the yellow and blue regions represent charge accumulation and depletion, respectively).

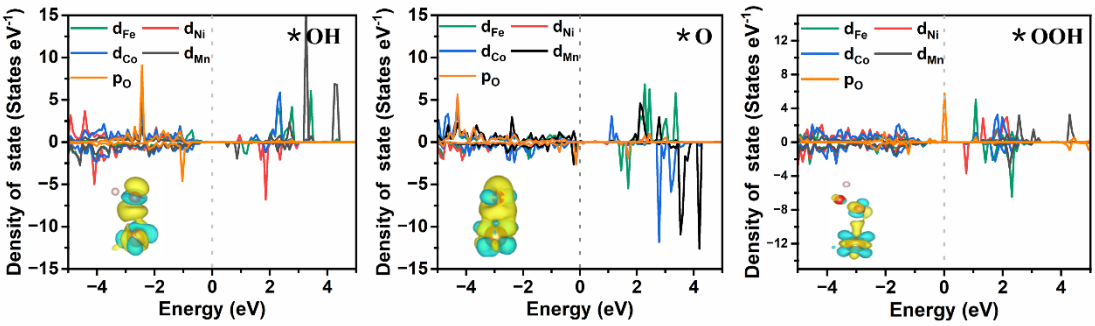

Fig. S21. DOS and charge density difference of the NiFe-rich HESO at *OH, *O, and *OOH adsorption step (the yellow and blue regions represent charge accumulation and depletion, respectively).

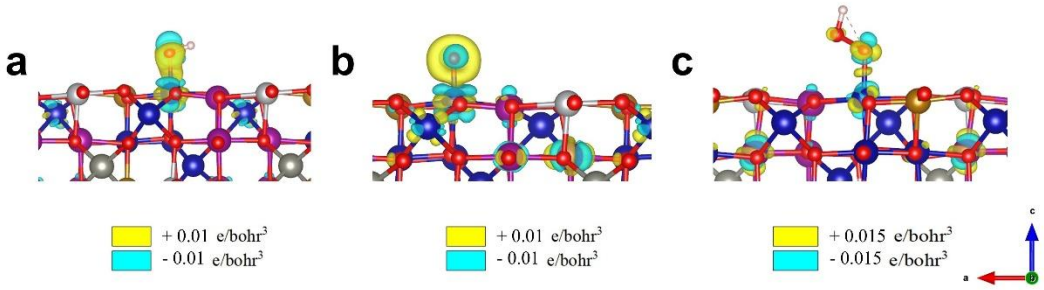

Figure S22. Charge density difference upon adsorption of (a) *OH, (b) *O, and (c) *OOH on CoMn-rich HESO. The yellow and blue regions represent charge accumulation and depletion, respectively.

Table S1. EDS data of HEOs (Atomic%)

		Fe	Ni	Co	Mn	Zn
Sample1	$(Ni_{0.2}Fe_{0.2}Co_{0.2}Mn_{0.2}Zn_{0.2})_3O_4$	**19.2**	**21.5**	**19.4**	**20.2**	**19.6**
Sample2	**NiFe-rich**	**36.5**	**30.2**	**11.3**	**11.1**	**10.9**
Sample3	**CoMn-rich**	**12.1**	**11.9**	**32.9**	**33.1**	**9.9**

Table S2. Comparison of OER performance of different transition metal-based catalysts.

Catalysts	Overpotential at 10 mA cm^{-2} (mV)	Tafel slope (mV Dec^{-1})	Durability	Ref
$(CoNiMnZnFe)_3O_{3.2}$	336	47.5	20h @ 10 mA cm^{-2}	1
$(CoCuFeMnNi)_3O_4$	400	76.7	12h @ 10 mA cm^{-2}	2
$La(CrMnFeCo_2Ni)O_3$	325	51.2	50h @ 10 mA cm^{-2}	3
$(MgFeCoNiCu)_3O_4$	300	40.0	25h @ 10 mA cm^{-2}	4
$Co_3O_{3.87}F_{0.13}$	440	56	1500 cycles	5
$CoMn_2O_4$/NCNFs	340	93.5	10h @ 10 mA cm^{-2}	6
$CoFe_2O_4$/CNTs	520	133	60h @ 10 mA cm^{-2}	7
$(Fe_{0.2}Co_{0.2}Ni_{0.2}Cu_{0.2}Zn_{0.2})Al_2O_4$	400	—	5h @ 10 mA cm^{-2}	8
n-Co_3O_4	380	153	—	9
$CaFe_2O_4$	350	50	100 cycles	10
$Mg_{0.2}Co_{0.2}Ni_{0.2}Cu_{0.2}Zn_{0.2}O$	360	61.4	25h @10 mA cm^{-2}	11
$CoMn(NiFeZn)O_4$	330.1	53.5	120h @10 mA cm^{-2}	This work

Table S3. Ratio of different valence states of each element in XPS.

	Fe (%)	Ni (%)	Co (%)	Mn (%)	Zn (%)
	2+:3+	2+:3+	2+:3+	2+:3+	2+
$(Ni_{0.2}Fe_{0.2}Co_{0.2}Mn_{0.2}Zn_{0.2})_3O_4$	51:49	60:40	42:58	47:53	100
NiFe-rich	62:38	58:42	46:54	47:53	100
CoMn-rich	49:51	59:41	29:71	49:51	100

Table S4. Ratio of O_I, O_{II}, and O_{III} in the CoMn-rich, NiFe-rich, and equimolar samples.

	O_I (%)	O_{II} (%)	O_{III} (%)
$(Ni_{0.2}Fe_{0.2}Co_{0.2}Mn_{0.2}Zn_{0.2})_3O_4$	68.07	25.58	6.34
NiFe-rich	68.72	20.65	10.63
CoMn-rich	46.38	32.35	21.27

Table S5. Ratio of O_I, O_{II}, and O_{III} in the CoMn-rich, NiFe-rich, and equimolar samples after Ar^+ sputtering.

	O_I (%)	O_{II} (%)	O_{III} (%)
$(Ni_{0.2}Fe_{0.2}Co_{0.2}Mn_{0.2}Zn_{0.2})_3O_4$	70.4	29.6	-
NiFe-rich	74.1	25.9	-
CoMn-rich	64.9	35.1	-

Reference

1. Y. Zhang, W. Dai, P. Zhang, T. Lu and Y. Pan, *J. Alloys Compd.*, 2021, **868**, 159064.
2. D. Wang, Z. Liu, S. Du, Y. Zhang, H. Li, Z. Xiao, W. Chen, R. Chen, Y. Wang and Y. Zou, *Journal of Materials Chemistry A*, 2019, **7**, 24211-24216.
3. T. X. Nguyen, Y. C. Liao, C. C. Lin, Y. H. Su and J. M. Ting, *Adv. Funct. Mater.*, 2021, **31**, 2101632.
4. T. X. Nguyen, Z.-T. Huang and J.-M. Ting, *Appl. Surf. Sci.*, 2021, **570**, 151160.
5. H. Zeng, X. Zhong, N. Alonso-Vante, F. Du, Y. Xie, Y. Huang and J. Ma, *Appl. Catal., B*, 2021, **281**, 119535.
6. X. Chen, Z. Yan, M. Yu, H. Sun, F. Liu, Q. Zhang, F. Cheng and J. Chen, *Journal of Materials Chemistry A*, 2019, **7**, 24868-24876.
7. T. Zhang, Z. Li, L. Wang, Z. Zhang and S. Wang, *Int. J. Hydrogen Energy*, 2019, **44**, 1610-1619.
8. R. R. Katzbaer, F. M. dos Santos Vieira, I. Dabo, Z. Mao and R. E. Schaak, *J. Am. Chem. Soc.*, 2023, **145**, 6753-6761.
9. C. Alex, S. C. Sarma, S. C. Peter and N. S. John, *ACS Applied Energy Materials*, 2020, **3**, 5439-5447.
10. Y. Sugawara, K. Kamata, A. Ishikawa, Y. Tateyama and T. Yamaguchi, *ACS Applied Energy Materials*, 2021, **4**, 3057-3066.
11. F. Liu, M. Yu, X. Chen, J. Li, H. Liu and F. Cheng, *Chinese Journal of Catalysis*, 2022, **43**, 122-129.